Mitofusin 2 ablation increases endoplasmic reticulum–mitochondria coupling

Riccardo Filadi[a], Elisa Greotti[a,b], Gabriele Turacchio[c], Alberto Luini[c], Tullio Pozzan[a,b,d,1], and Paola Pizzo[a,1]

[a]Department of Biomedical Sciences, University of Padua, Padua, 35121, Italy; [b]Department of Biomedical Sciences, Institute of Neuroscience (Padua Section), Italian National Research Council, Padua, 35121, Italy; [c]Department of Biomedical Sciences, Institute of Protein Biochemistry, Italian National Research Council, Naples, 80131, Italy; and [d]Venetian Institute of Molecular Medicine, Padua, 35121, Italy

Contributed by Tullio Pozzan, March 13, 2015 (sent for review January 9, 2015; reviewed by Dalton J. Surmeier)

The organization and mutual interactions between endoplasmic reticulum (ER) and mitochondria modulate key aspects of cell pathophysiology. Several proteins have been suggested to be involved in keeping ER and mitochondria at a correct distance. Among them, in mammalian cells, mitofusin 2 (Mfn2), located on both the outer mitochondrial membrane and the ER surface, has been proposed to be a physical tether between the two organelles, forming homotypic interactions and heterocomplexes with its homolog Mfn1. Recently, this widely accepted model has been challenged using quantitative EM analysis. Using a multiplicity of morphological, biochemical, functional, and genetic approaches, we demonstrate that Mfn2 ablation increases the structural and functional ER–mitochondria coupling. In particular, we show that in different cell types Mfn2 ablation or silencing increases the close contacts between the two organelles and strengthens the efficacy of inositol trisphosphate (IP3)-induced Ca^{2+} transfer from the ER to mitochondria, sensitizing cells to a mitochondrial Ca^{2+} overload-dependent death. We also show that the previously reported discrepancy between electron and fluorescence microscopy data on ER–mitochondria proximity in Mfn2-ablated cells is only apparent. By using a different type of morphological analysis of fluorescent images that takes into account (and corrects for) the gross modifications in mitochondrial shape resulting from Mfn2 ablation, we demonstrate that an increased proximity between the organelles is also observed by confocal microscopy when Mfn2 levels are reduced. Based on these results, we propose a new model for ER–mitochondria juxtaposition in which Mfn2 works as a tethering antagonist preventing an excessive, potentially toxic, proximity between the two organelles.

mitofusin 2 | ER–mitochondria tethering | inter-organellar communication

During the last decade, evidence has accumulated showing the existence of a continuous flux of information between the endoplasmic reticulum (ER) and mitochondria, two organelles whose privileged interplay is essential, e.g., for lipid metabolism and modulation of Ca^{2+} signaling (1, 2). As to the former, Vance (3) firstly described a partially purified microsomal subfraction pulled down with mitochondria (fraction X, later renamed "mitochondria-associated membrane," MAM) that was found to be enriched in phosphatidylserine synthase and several enzymes involved in lipid and glucose metabolism, cholesterol, and ceramide biosynthesis (4, 5). As far as Ca^{2+} signaling is concerned, the ER–mitochondria axis plays a critical role in cell Ca^{2+} homeostasis (6–8). In parallel, increases of Ca^{2+} within mitochondria are essential in tuning physiological organelle activity (9, 10) and in modulating the process of cell death (6, 8, 11). ER–mitochondria connections and Ca^{2+} signals are also critical for mitochondrial fission (12, 13), for autophagosome generation (14), and for the removal of damaged mitochondria by autophagy (15).

Several proteins have been suggested to be involved in maintaining a given distance between ER and mitochondria (16), allowing their correct organization, mutual interactions, and Ca^{2+} cross talk (17). In mammalian cells, mitofusin 2 (Mfn2), located on both the outer mitochondrial membrane (OMM) and the ER surface, has been proposed to take part at the level of MAMs in homotypic interactions, and heterocomplexes engaging the Mfn2 homolog Mfn1 on mitochondria, that may contribute to ER–mitochondria tethering (18). Recently, however, this widely accepted model has been challenged by a quantitative EM analysis showing an increase, not a decrease, in the close contacts between the two organelles in *Mfn2*$^{-/-}$ cells, as compared with WT cells (19). No explanation has been proposed so far for the contradictory EM and fluorescence data or for the reduced transfer of Ca^{2+} from the ER to mitochondria upon activation of IP3 receptors in *Mfn2*$^{-/-}$ MEFs (18).

We here show that the discrepancy between these data is only apparent and that cells in which Mfn2 is ablated (*Mfn2*$^{-/-}$) or silenced (Mfn2-KD) display increased ER–mitochondria tethering, strengthened ER–mitochondria Ca^{2+} transfer, and greater sensitivity to apoptotic stimuli linked to mitochondrial Ca^{2+} overload toxicity. Based on these experimental data, we propose a revised model for ER–mitochondria tethering in which Mfn2 negatively modulates the number of close contacts between the two organelles. Conditions or treatments that decrease Mfn2 expression remove its negative control on tethering, boosting potentially toxic ER–mitochondria cross talk.

Results

Mfn2 Ablation/Reduction Increases ER–Mitochondria Physical Proximity. To investigate in detail the role played by Mfn2 in ER–mitochondria physical interaction, we carried out quantitative EM analyses of cells in which Mfn2 was ablated or transiently reduced by an siRNA-based technique. We found a net increase in the

Significance

The privileged interrelationship between mitochondria and the endoplasmic reticulum (ER) plays a key role in a variety of physiological functions, from lipid metabolism to Ca^{2+} signalling, and its modulation influences apoptotic susceptibility, mitophagy, and cellular bioenergetics. Among the several proteins known to influence ER–mitochondria interactions, mitofusin 2 (Mfn2) has been proposed to form a physical tether. In this study, we demonstrate that Mfn2 instead works as an ER–mitochondria tethering antagonist preventing an excessive, potentially toxic, proximity between the two organelles. Cells in which Mfn2 is ablated or reduced have an increased number of ER–mitochondria close contacts, potentiated Ca^{2+} transfer between the two organelles, and greater sensitivity to cell-death stimuli that implies mitochondria Ca^{2+} overload toxicity.

Author contributions: T.P. and P.P. designed research; R.F., E.G., and G.T. performed research; R.F., E.G., G.T., and A.L. analyzed data; and T.P. and P.P. wrote the paper.

Reviewers included: D.J.S., Northwestern University.

The authors declare no conflict of interest.

Freely available online through the PNAS open access option.

[1]To whom correspondence may be addressed. Email: tullio.pozzan@unipd.it or paola.pizzo@unipd.it.

This article contains supporting information online at www.pnas.org/lookup/suppl/doi:10.1073/pnas.1504880112/-/DCSupplemental.

number of close (≤15 nm) contacts between ER and mitochondria in *Mfn2*$^{-/-}$ mouse embryonic fibroblasts (MEFs) as compared with WT MEFs (Fig. 1 *A* and *B*, *Right*) and electron-dense "bridges" in the regions of close apposition between the organelles (Fig. 1*B*, *Left*). The result was not merely a clonal feature of *Mfn2*$^{-/-}$ cells: The number of close appositions between ER and mitochondria increased in WT MEFs acutely knocked down for Mfn2 by specific siRNAs (Fig. S1) as compared with controls (Fig. 1*B*, *Right*, and Fig. 1*C*). Of note, Mfn2 ablation does not modify the averaged extension of each contact significantly (110.35 ± 10.17 nm and 138.03 ± 12.82 nm in WT and *Mfn2*$^{-/-}$ MEFs, respectively, mean ± SEM of three independent experiments). In addition, a reduction in the number of mitochondria was observed in both *Mfn2*$^{-/-}$ and Mfn2-KD cells as compared with controls (average number of mitochondria per cell ± SEM: 24.5 ± 2.14 in WT MEFs vs. 15.4 ± 1.69 in *Mfn2*$^{-/-}$ MEFs, $P < 0.01$, $n = 30$ and 20 cells, respectively; for control and Mfn2-KD cells: 24.1 ± 3.77 and 12.4 ± 2.78, respectively, $P < 0.05$, $n = 10$ cells). Our results thus confirm and extend the findings of Cosson et al. (19), compelling more detailed studies on the tethering role of Mfn2. Moreover, a close inspection of EM micrographs revealed that, in addition to the classical close contacts, long-distance (50–100 nm) regions of apposition between ER and mitochondria (with a mean length extension of 250 nm; Fig. S2) are also observed. However, a correlation between their number and the presence of Mfn2 has not been found. In particular, although the number of these "loose" contacts was lower in *Mfn2*$^{-/-}$ MEFs than in controls, no significant difference was observed between cells treated with Mfn2-specific siRNAs and their controls, suggesting that these structures are independent of Mfn2 and likely result from some clonal adaptations.

In apparent contradiction to the EM observations, confocal microscopy analyses of fixed cells expressing two fluorescent proteins (an ER-GFP and a mitochondrial RFP, hereafter "mit-RFP") in both stable *Mfn2*$^{-/-}$ MEFs and Mfn2-KD MEFs revealed a net decrease in the overlapping area between ER and mitochondria (Fig. 2 *A* and *B*), confirming and extending data previously reported (18). We obtained similar colocalization results in living cells (Pearson's coefficients of 0.268 ± 0.018 and 0.081 ± 0.023 and Manders' coefficients of 0.521 ± 0.014 and 0.321 ± 0.017 in WT and *Mfn2*$^{-/-}$ MEFs, respectively; $P < 0.01$, $n = 18$ and 21 cells, respectively) and with a different fixation protocol (the same used for EM; Pearson's coefficients of 0.208 ± 0.019 and 0.068 ± 0.027; Manders' coefficients of 0.529 ± 0.016 and 0.370 ± 0.024, in WT and *Mfn2*$^{-/-}$ MEFs, respectively; $P < 0.01$, $n = 20$ and 17 cells, respectively), thus excluding the possibility that differences between EM and confocal microscopy results were caused by artifacts linked to different methods of sample preparation.

Trying to explain this discrepancy, we reasoned that, in addition to the very different spatial resolution of the two techniques, EM and fluorescence microscopy differ in that EM evaluates the number and size of the contacts between the perimeters of the organelles, whereas fluorescence microscopy usually is carried out using luminal fluorescent proteins; accordingly, the colocalization algorithms provide a measure of the overlapping areas/volumes of ER and mitochondria. This difference is irrelevant when the applied treatments or genetic manipulations do not markedly modify the morphology of the organelles. However, given the resolution of fluorescence microscopy, if the area of the organelles increases more markedly than the perimeter (e.g., in mitochondrial swelling), this differential increase could result in an apparent decrease in ER–mitochondria tethering (see Fig. 2*C* for an artificial example of the phenomenon). In particular, it has been shown (and we confirmed here) that upon Mfn2 ablation or reduction there are marked changes in the mitochondrial shape (fragmentation and swelling with an increase in the mean length of the organelle minor axis) and a strong reduction in the cellular area occupied by the whole mitochondrial network (Fig. 3*A*, Fig. S1*B*, and Tables S1 and S2) that could make classical colocalization methods of analysis not suitable (20, 21). We thus chose a different approach to quantify organelles' colocalization (*Materials and Methods*), taking into consideration only the perimeter of the mitochondrial structures, not their entire area (Figs. 2*D* and 3*B*). Using this method, we found the percentage of the mitochondrial perimeter colocalizing with the ER increased, in accordance with the EM

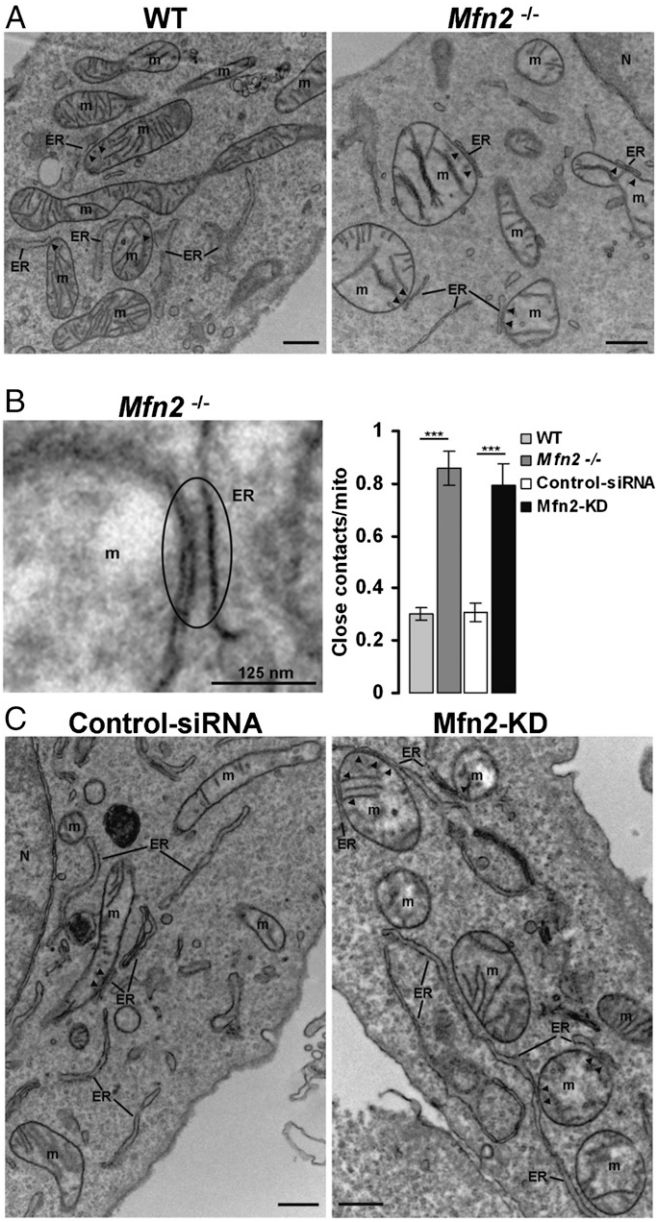

Fig. 1. Mfn2 ablation/reduction increases close contacts between ER and mitochondria. (*A* and *C*) Representative EM images of WT and *Mfn2*$^{-/-}$ MEFs (*A*) or control siRNA and Mfn2-KD MEFs (*C*). Several close appositions (≤15 nm, indicated by arrowheads) are visible between ER cisternae and mitochondria (m) in WT/control siRNA MEFs and, more frequently, in *Mfn2*$^{-/-}$ (*A*) or Mfn2-KD (*C*) MEFs. (Scale bars, 0.5 μm.) (*B*, *Left*) Representative enlarged EM image of electron-dense proteinaceous structures in the region of close apposition between the organelles in *Mfn2*$^{-/-}$ MEFs. (*Right*) Average number of close contacts per mitochondrion observed in WT, *Mfn2*$^{-/-}$, control siRNA, and Mfn2-KD MEFs. $n = 735$, 308, 253, and 165 mitochondria for WT, *Mfn2*$^{-/-}$, control siRNA, and Mfn2-KD MEFs, respectively; results shown are the mean ± SEM of three independent experiments; ***$P < 0.001$.

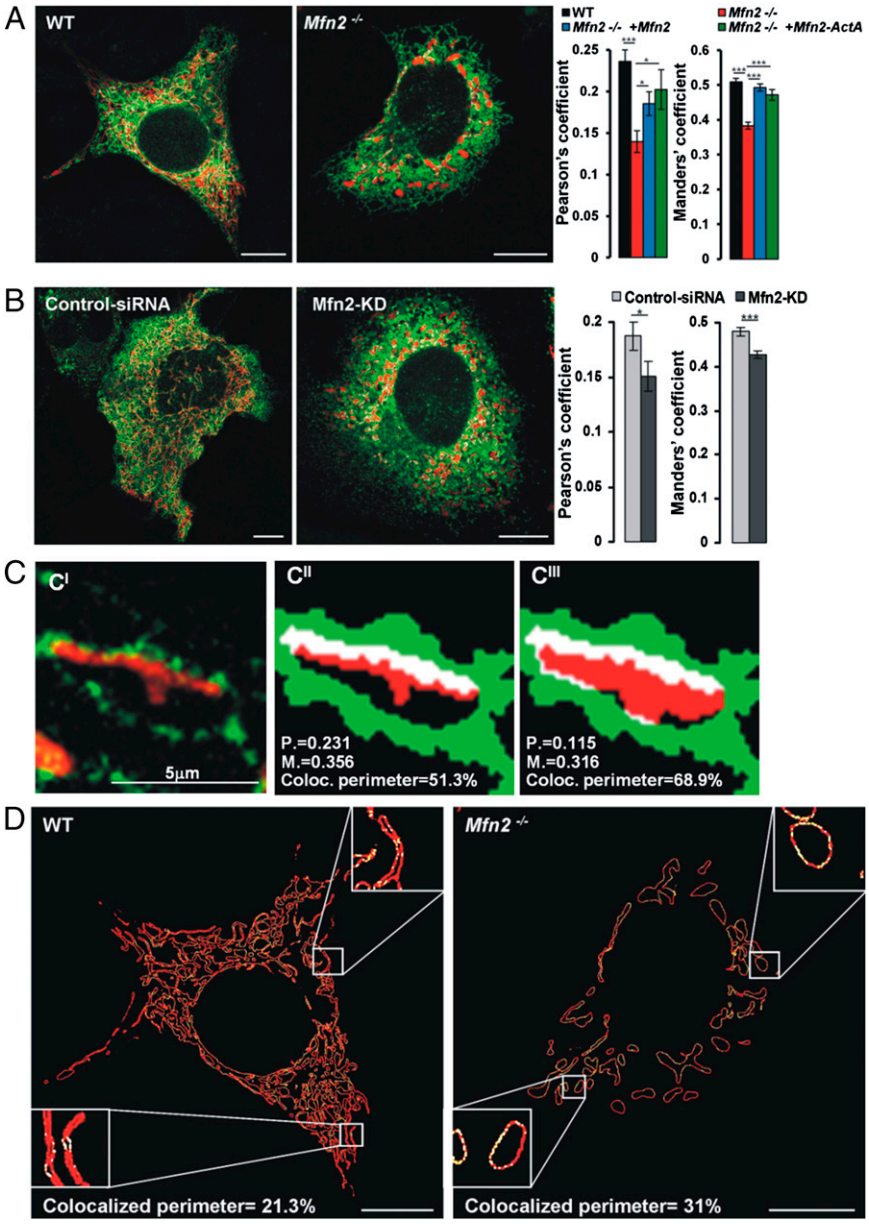

Fig. 2. ER–mitochondria colocalization analysis in Mfn2$^{-/-}$ and Mfn2-KD MEFs. (*A* and *B*) ER–mitochondria interactions in WT and *Mfn2*$^{-/-}$ (*A*) and control siRNA and Mfn2-KD (*B*) MEFs upon expression of mit-RFP and ER-GFP, as shown by confocal microscopy. (Scale bars, 10 μm.) Manders' and Pearson's coefficients are shown for each condition. $n = 51$, 68, 25, 14, 75, and 80 cells for WT, *Mfn2*$^{-/-}$, *Mfn2*$^{-/-}$ + Mfn2, *Mfn2*$^{-/-}$ + Mfn2^{ActA}, control siRNA, and Mfn2-KD MEFs, respectively. Results shown are the mean ± SEM of four independent experiments; $*P < 0.05$; $***P < 0.001$. (*C*) The cartoon shows how marked changes in the mitochondrial area could result in an artificial decrease in the classical Mander's (M.) and Pearson's (P.) colocalization coefficients. (*C′*) Cropped fluorescence image (from a HeLa cell expressing mit-RFP and ER-GFP) showing a mitochondrion in contact with the ER. (*C″* and *C‴*) Artificial reproductions of the image in *C′* showing that M. and P. coefficients are decreased upon mitochondrial swelling (*C‴*), although the percentage of mitochondrial perimeter in contact with the ER (Coloc. perimeter) is increased. (*D*) The images in *A* were analyzed with the perimeter plugin (*Materials and Methods*). Red pixels correspond to the whole mitochondrial perimeter profiles; yellow pixels represent the points in which the mitochondrial perimeter is in contact with the ER. Enlarged regions show increased perimeter colocalization (yellow pixels) in *Mfn2*$^{-/-}$ MEFs.

data, in both *Mfn2*$^{-/-}$ and Mfn2-KD MEFs as compared with controls (Fig. 3*C*) and that the reintroduction of Mfn2 in *Mfn2*$^{-/-}$ MEFs rescued the mitochondrial morphology (Fig. 3*A*) and decreased the percentage of mitochondrial perimeter colocalized with the ER (Fig. 3*C*). Importantly, the expression of a "mitochondrial only" Mfn2 (Mfn2^{ActA}) (18) in *Mfn2*$^{-/-}$ MEFs, which should not modify ER–mitochondria tethering while completely restoring organelles' morphology (18), increases classical colocalization indexes (Fig. 2*A*) but does not significantly modify the extent of the ER–mitochondria overlapping regions as calculated on the organelles' perimeter (Fig. 3*C*). On the other hand, when the presenilin 2 (PS2) familial Alzheimer disease mutant PS2-T122R was expressed in HeLa cells [a treatment shown to increase ER–mitochondria physical and functional coupling without altering organelles' morphology (Fig. S3*A*) (22)], both types of analysis showed an increase in the organelles' colocalization (Fig. S3*B*). Thus, for a correct evaluation of organelles' surface apposition, classical Manders' and Pearson's colocalization coefficients appear to be useful tools when no marked changes in organelles' morphology occur; in other

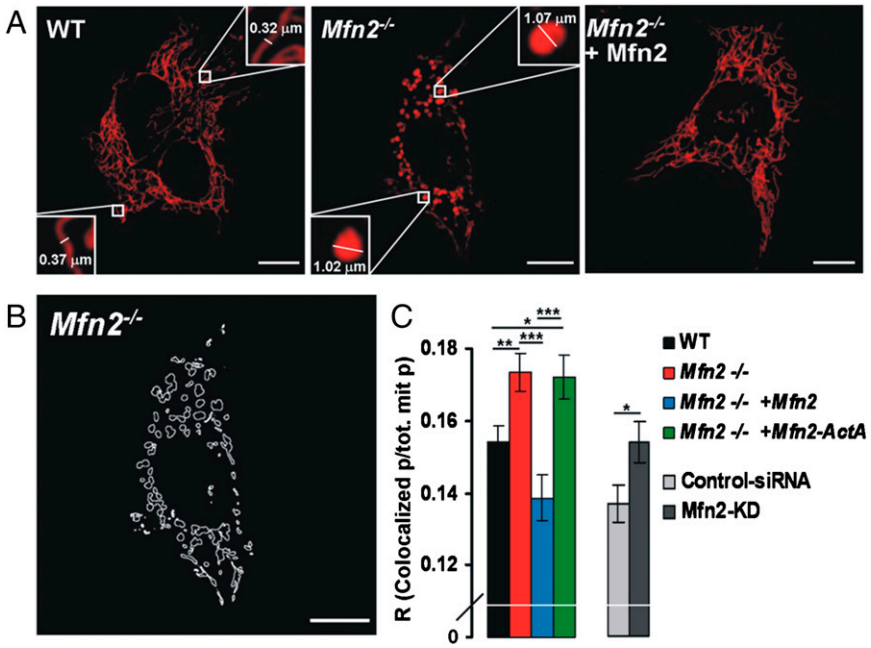

Fig. 3. Mfn2 ablation/reduction increases ER–mitochondria surface juxtaposition. (*A*) Representative fluorescence images of the indicated MEF types expressing mit-RFP. Enlarged regions show the increased dimension of the minor axis of individual mitochondria. (Scale bars, 10 μm.) (*B*) Representative mitochondrial perimeter profile of the *Mfn2*$^{-/-}$ cell shown in *A*. (*C*) ER–mitochondria signal colocalization indexes, calculated as the ratio (R) between mitochondrial perimeter pixels colocalized with the ER and total mitochondrial perimeter pixels (*Materials and Methods*) for the indicated MEF types ($n = 51$, 68, 25, 14, 75, and 80 cells for WT, *Mfn2*$^{-/-}$, *Mfn2*$^{-/-}$ + Mfn2, *Mfn2*$^{-/-}$ + Mfn2^{ActA}, control siRNA, and Mfn2-KD MEFs, respectively). Data shown represent the mean ± SEM of four independent experiments; *$P < 0.05$; **$P < 0.01$; ***$P < 0.001$.

circumstances, an additional, specific type of analysis is required (21).

Mfn2 Down-Regulation Increases ER–Mitochondria Ca^{2+} Cross Talk. From a functional point of view, conditions that induce an increased apposition of the two organelles should favor the uptake of Ca^{2+} by mitochondria upon Ca^{2+} release from the ER, a process that depends largely on the formation of Ca^{2+} hot spots in regions where the two organelles are sufficiently close (23, 24). Nevertheless, when we used cytosolic-targeted aequorin (cyt-Aeq) or mitochondria-targeted aequorin (mit-Aeq) as probes for Ca^{2+} responses to the IP_3-generating agonist ATP, MEF clones showed a decreased mitochondrial Ca^{2+} uptake in *Mfn2*$^{-/-}$ cells as compared with WT MEFs (Fig. S4) (18).

However, the efficacy of ER–mitochondria Ca^{2+} transfer upon an IP_3-generating stimulus depends not only on the distance between the organelles but also on the level of expression of the mitochondrial Ca^{2+} uptake machinery. Therefore we measured the expression level of the pore-forming subunit of the mitochondrial Ca^{2+} uniporter (MCU) (25, 26). The MCU was reduced by about 50% in *Mfn2*$^{-/-}$ cells as compared with controls (Fig. 4*A*). Therefore, the reduced mitochondrial Ca^{2+} uptake in *Mfn2*$^{-/-}$ cells is solely the result of MCU down-regulation. This conclusion is confirmed by the observation that, in the same cells permeabilized with digitonin and perfused with medium at fixed $[Ca^{2+}]$ (*Materials and Methods*), the rates and peaks of mitochondrial Ca^{2+} uptake are substantially reduced as compared with WT MEFs (Fig. 4*B*). Under these conditions, the ER Ca^{2+} is completely depleted, and no Ca^{2+} hot spots are generated on the mitochondrial surface (23).

The opposite strategy, i.e., Mfn2 overexpression in WT cells, cannot be used to investigate the role of the protein in ER–mitochondria coupling, because this approach induces mitochondrial fragmentation and aggregation (Fig. S5 and Table S2), leading to mitochondrial dysfunction and cell death (27–29).

Therefore we next investigated the effect of acute down-regulation of Mfn2. Importantly, in this case we observed no difference in MCU expression levels compared with controls (Fig. 4*A*), while, in response to stimulations with ATP, which cause similar $[Ca^{2+}]_{cyt}$ rises in control siRNA and Mfn2-KD cells (Fig. 4*D*, *Inset*), the $[Ca^{2+}]_{mit}$ peaks of Mfn2-KD MEFs were substantially higher (Fig. 4*D*), suggesting that this condition favors Ca^{2+} transfer from the ER to mitochondria. In support of the conclusion that the increased mitochondrial Ca^{2+} uptake in response to an IP_3-induced Ca^{2+} release is caused by an increased number of ER–mitochondria appositions, control siRNA and Mfn2-KD cells showed very similar $[Ca^{2+}]_{mit}$ increases upon plasma membrane permeabilization and perfusion with fixed $[Ca^{2+}]$ (Fig. 4*C*). The phenomenon was siRNA and cell-type independent, since it was also observed in Mfn2-KD SH-SY5Y cells using a different, human-targeted siRNA (Fig. S6). Importantly, the potentiation of ER–mitochondria Ca^{2+} cross talk observed in Mfn2-KD MEFs was abolished by Mfn2 reexpression (Fig. 4*D* and Fig. S1*A*).

Because Mfn2 ablation/reduction causes gross mitochondrial morphological alterations, we wondered whether such conditions could induce changes in mitochondrial bioenergetics that might contribute to the different mitochondrial Ca^{2+} responses we observed. We thus evaluated mitochondrial membrane potential, oxygen consumption, and cellular ATP levels in WT and Mfn2-KD MEF cells, avoiding the direct comparison of different MEF clones (WT and *Mfn2*$^{-/-}$) because they are prone to adaptation phenomena (see above). Respiration and ATP levels are indistinguishable in control and Mfn2-KD cells, although a marginal reduction in mitochondrial tetramethyl rhodamine methyl ester (TMRM) fluorescence was found in Mfn2-KD cells (Fig. S7). Overall, Mfn2 deficiency has no, or only a very modest, direct effect on mitochondrial bioenergetics (as also suggested by the measurement of mitochondrial Ca^{2+} uptake in permeabilized cells; Fig. 4*C*).

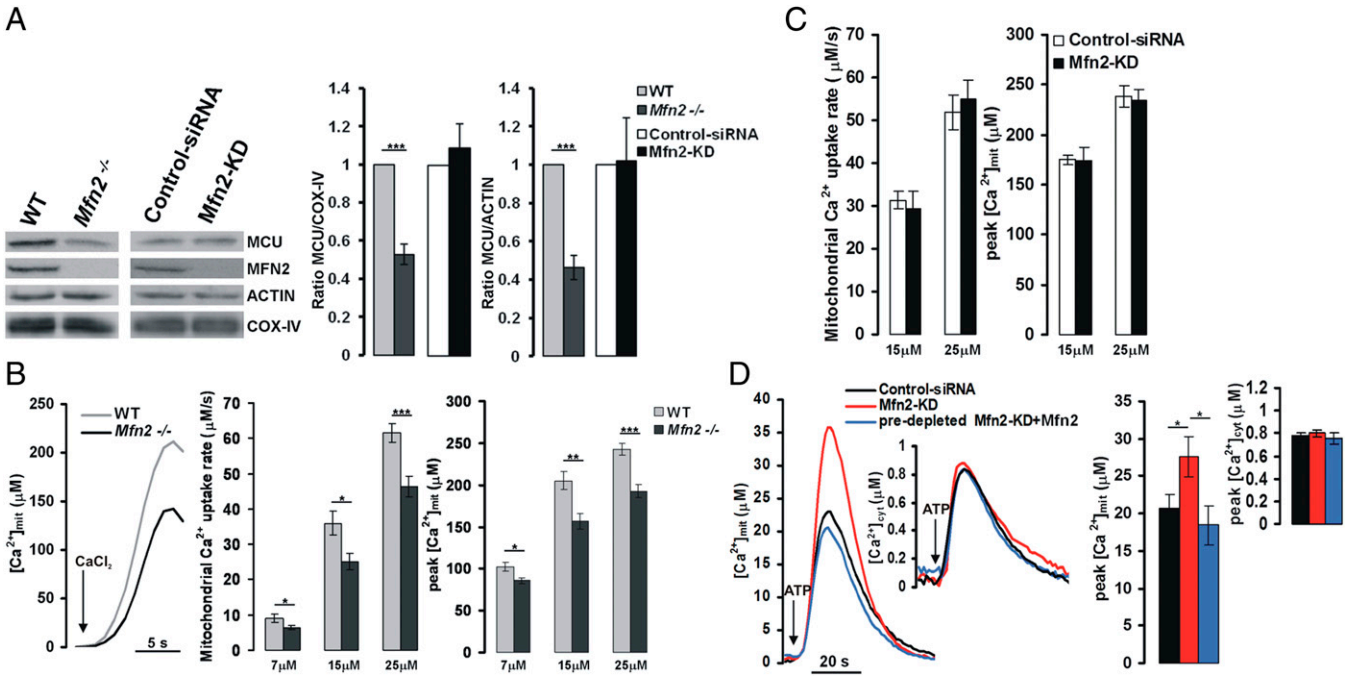

Fig. 4. Mfn2 down-regulation increases ER–mitochondria Ca^{2+} transfer. (*A*, *Left*) MCU, MFN2, Actin and COX-IV expression levels in the indicated MEF types. (*Right*) Ratios (R) of the level of MCU expression and the level of COX-IV or actin protein in the different MEF types normalized to controls. Data shown represent the mean ± SEM of five independent experiments. ***$P < 0.001$. (*B*) $[Ca^{2+}]_{mit}$ peaks (*Right*) and maximal Ca^{2+} uptake rate (*Middle*) obtained in MEFs of the indicated genotypes upon permeabilization of the plasma membrane with digitonin and perfusion with an intracellular-like medium containing different (7, 15, or 25 μM) fixed $[Ca^{2+}]$. Representative traces (*Left*) of WT and *Mfn2*$^{-/-}$ cells are shown upon the addition of 15 μM $[Ca^{2+}]$. Data shown represent the mean ± SEM of 13, 12, and 9 independent experiments for $[Ca^{2+}]$ concentrations of 7, 15, and 25 μM, respectively, *$P < 0.05$; **$P < 0.01$; ***$P < 0.001$. (*C*) $[Ca^{2+}]_{mit}$ peaks (*Right*) and maximal Ca^{2+} uptake rate (*Left*) obtained in permeabilized control siRNA and Mfn2-KD MEFs obtained as in *B*. Data shown represent the mean ± SEM of six independent experiments for each condition. (*D*) $[Ca^{2+}]_{mit}$ (*Left*) and $[Ca^{2+}]_{cyt}$ (*Left*, *Inset*) changes in intact control siRNA and Mfn2-KD MEFs. Representative cytosolic and mitochondrial Ca^{2+} traces in control siRNA (black), Mfn2-KD (red), and predepleted Mfn2-KD+Mfn2 (blue) MEFs bathed in Ca^{2+}-free, EGTA-containing medium and challenged with 200 μM ATP. (*Right*) Mean $[Ca^{2+}]_{mit}$ and $[Ca^{2+}]_{cyt}$ (*Right*, *Inset*) peaks upon ATP stimulation in the different conditions. For cytosolic Ca^{2+} measurements, data shown represent the mean ± SEM of 14, 18, and 5 independent experiments for control siRNA, Mfn2-KD, and predepleted Mfn2-KD+Mfn2 MEFs, respectively. For mitochondrial Ca^{2+} measurements, the data shown represent the mean ± SEM of 17, 19, and 8 independent experiments for control siRNA, Mfn2-KD, and predepleted Mfn2-KD+Mfn2 MEFs, respectively. *$P < 0.05$.

Mfn2 Ablation Does Not Alter the Dynamics of ER–Mitochondria Interactions. To characterize better the role of Mfn2 in ER–mitochondria contacts, we decided to monitor their dynamics in WT or *Mfn2*$^{-/-}$ living MEFs expressing an ER-GFP and a mit-RFP. Indeed, as previously observed in other cell types (30), despite their continuous rearrangements, ER and mitochondria are persistently kept in contact in specific regions over time. We observed that in *Mfn2*$^{-/-}$ MEFs, as in WT cells, when both organelles are moving, the dynamics of a mitochondrion in the cell periphery (where the ER is better resolved) are tightly coordinated, interconnected, and maintained with those of the corresponding neighbor ER tubule (Fig. 5*A* and Movie S1). We reasoned that the dynamic analysis of the ER–mitochondria colocalization profile (calculated from the entire cell, as described above, considering only the mitochondrial perimeter; Figs. 2*D* and 3 *B* and *C*) could provide additional information about the stability of the contacts between the two organelles. Indeed, if contacts (white overlapping pixels in Fig. 5*A*) are unstable or accidental, a variable, inconstant profile should be obtained; vice versa, whenever contacts are maintained over time, a more constant, nonoscillating profile is expected as outcome of the analysis. As shown in Fig. 5*C*, *Left*, the overlapping pixel profiles obtained over time from the entire cell (calculated as described in Fig. 5*B*; also see *Materials and Methods*) were found to be indistinguishable between WT and *Mfn2*$^{-/-}$ cells, suggesting that, despite their increased number, the stability of the contacts is unaffected by the absence of Mfn2 and thus further challenging the model of an Mfn2-based tether between the two organelles. To validate the assay, a synthetic ER–mitochondria linker known to cause tighter and wider organelles associations (31) was expressed in WT MEFs. This artificial linker, which formed a single-protein bridge connecting the OMM and the ER, stably forced the two organelles together. As predicted, the overlapping pixel profiles over time show a 30% reduction in the oscillations of the colocalization signal as compared with control cells expressing a truncated linker inserted only in the OMM but not bound to the ER (OMM-RFP) (Fig. 5*C*, *Right*).

Mfn2 Down-Regulation Increases ER and Mitochondria Membrane Association and Leads to Higher Sensitivity to Mitochondrial Ca^{2+}-Dependent Cell Death. We further biochemically evaluated the association of the two organelles by quantifying, after partial mitochondria purification by differential centrifugation, the MAMs that remain associated with them (17). The amount of ER proteins contaminating crude mitochondria fractions is an indirect value of the ER–mitochondria physical association. In this case, as in the experiments described in Fig. 4, we avoided directly comparing WT and *Mfn2*$^{-/-}$ MEFs because cell clones frequently are prone to adaptive phenomena that can lead to changes in the total expression levels of several proteins without any correlation with the molecule under investigation (see the previous discussion of MCU and Fig. 4*A*). Fig. 6*A* shows the results obtained in crude mitochondria isolated from WT MEFs in which Mfn2 was acutely down-regulated by a specific siRNA: When their total expression level is considered, all the ER/MAM proteins tested were enriched in Mfn2-KD mitochondrial fractions, as compared with

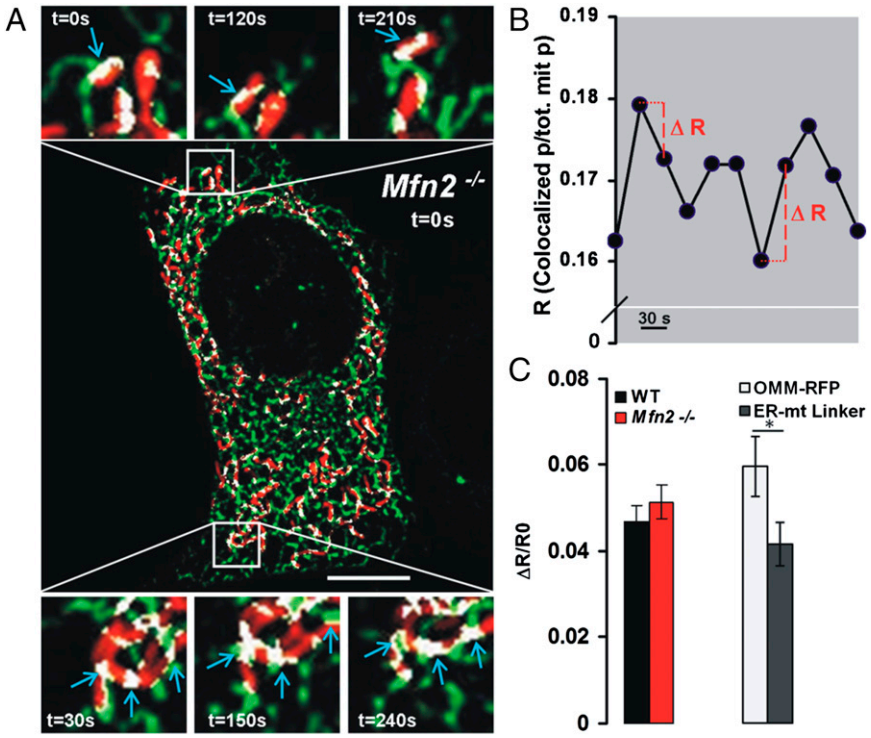

Fig. 5. Mfn2 ablation does not alter the dynamic of ER–mitochondria contacts. (*A*) Fluorescence image (modified as described in *Materials and Methods*) of a mit-RFP– and ER-GFP–expressing *Mfn2*$^{-/-}$ MEF with enlarged regions (boxes) corresponding to a time-lapse imaging of its stable ER–mitochondria interactions (white pixels indicated by cyan arrows) at the indicated time points (see also Movie S1). (Scale bar, 10 μm.) (*B*) Kinetics of the ratio (R, calculated as described in Fig. 3) on the entire *Mfn2*$^{-/-}$ cell shown in *A* but without any image modification. ΔR represents the difference between the R of one image (frame) and that of the previous one; frames were taken every 30 s; only two ΔRs are shown as an example. (*C*) Mean ΔR/R0 values (where R0 is the R of the first frame of each pair) of 100 frames from 10 different WT or *Mfn2*$^{-/-}$ MEF cells (*Left*) or of 60 frames from six different WT MEF cells expressing either an OMM-RFP (as control) or an artificial ER–mitochondrial linker (*Right*) (*SI Materials and Methods*). Data are shown as mean ± SEM; **P* < 0.05.

controls, confirming an increased ER–mitochondria interaction upon Mfn2 down-regulation.

It has been proposed that mitochondrial Ca^{2+} uptake upon treatment with specific apoptotic stimuli can sensitize cells to a mitochondrial Ca^{2+} overload-dependent cell death associated with the release of cytochrome *c* from mitochondria (32). We found that the increased ER–mitochondria physical proximity and the increased mitochondrial Ca^{2+} uptake caused by Mfn2 down-regulation result in a greater sensitivity to apoptotic stimuli that imply a mitochondrial Ca^{2+} overload-dependent toxicity. In Mfn2-KD SH-SY5Y cells, the fraction of annexin-V^+ cells is increased markedly after treatment with C_2-ceramide (plus an IP_3-generating stimulation) (*Materials and Methods*) compared with the fraction found in control cells (Fig. 6 *B* and *C*). Moreover, cytochrome *c* release was also increased in these cells compared with controls, as revealed by the reduced colocalization indexes between its immuno-signal and that of a mit-RFP (*Materials and Methods* and Fig. 6*D*). On the other hand, when another cell-death stimulus such as etoposide, which acts independently of mitochondrial Ca^{2+} overload toxicity (33, 34), was applied to control and Mfn2-KD cells, no difference was found in the number of annexin-V^+ cells (Fig. 6*C*), strongly suggesting a causal relationship between Mfn2, ER–mitochondria Ca^{2+} transfer, and cell-death sensitivity.

Discussion

Despite recent EM evidence (19) demonstrating that Mfn2 ablation results in an increase of the tight contacts between ER and mitochondria, the idea that Mfn2 is the key molecular component tethering the two organelles continues to be widely accepted (16, 17, 35, 36). This classical model is based not only on morphological data obtained by confocal microscopy but also on functional evidence, in particular the reduced Ca^{2+} transfer from the ER to mitochondria in *Mfn2*$^{-/-}$ cells (18). Here, however, we demonstrate that reduced Ca^{2+} transfer is the result of the lower expression in the *Mfn2*$^{-/-}$ MEF clone of the molecule (MCU) responsible for mitochondrial Ca^{2+} uptake and is independent of ER–mitochondria juxtapositions.

To the best of our knowledge, no explanation has been provided so far for the reported discrepancy between EM and fluorescence data regarding the tether function of Mfn2 (19). Here we demonstrate that the contradiction between the two types of morphological data is only apparent and is the result of the gross morphological alterations caused by Mfn2 ablation/reduction. Indeed, if a different approach that takes morphological alterations into account is used to analyze the fluorescent images, an increased ER–mitochondria apposition upon Mfn2 ablation/reduction is seen.

Importantly, our findings clearly show that an increased apposition between the two organelles is found upon acute silencing of Mfn2, i.e., independently of any possible clonal characteristics. This conclusion is strongly supported by functional/biochemical data: (*i*) the ER–mitochondria Ca^{2+} transfer is increased by Mfn2 down-regulation; (*ii*) Mfn2 expression modulates the number but not the extension and the dynamics of ER–mitochondria connections, suggesting that their molecular composition may be unaffected by its presence; (*iii*) Mfn2 reduction results in an increased amount of ER vesicles associated with mitochondria in subcellular fractionation experiments; (*iv*) Mfn2 down-regulation sensitizes cells to a mitochondrial Ca^{2+} overload-dependent cell death.

It has been reported very recently that an impaired mitochondrial respiratory capacity (caused by coenzyme Q reduction) is

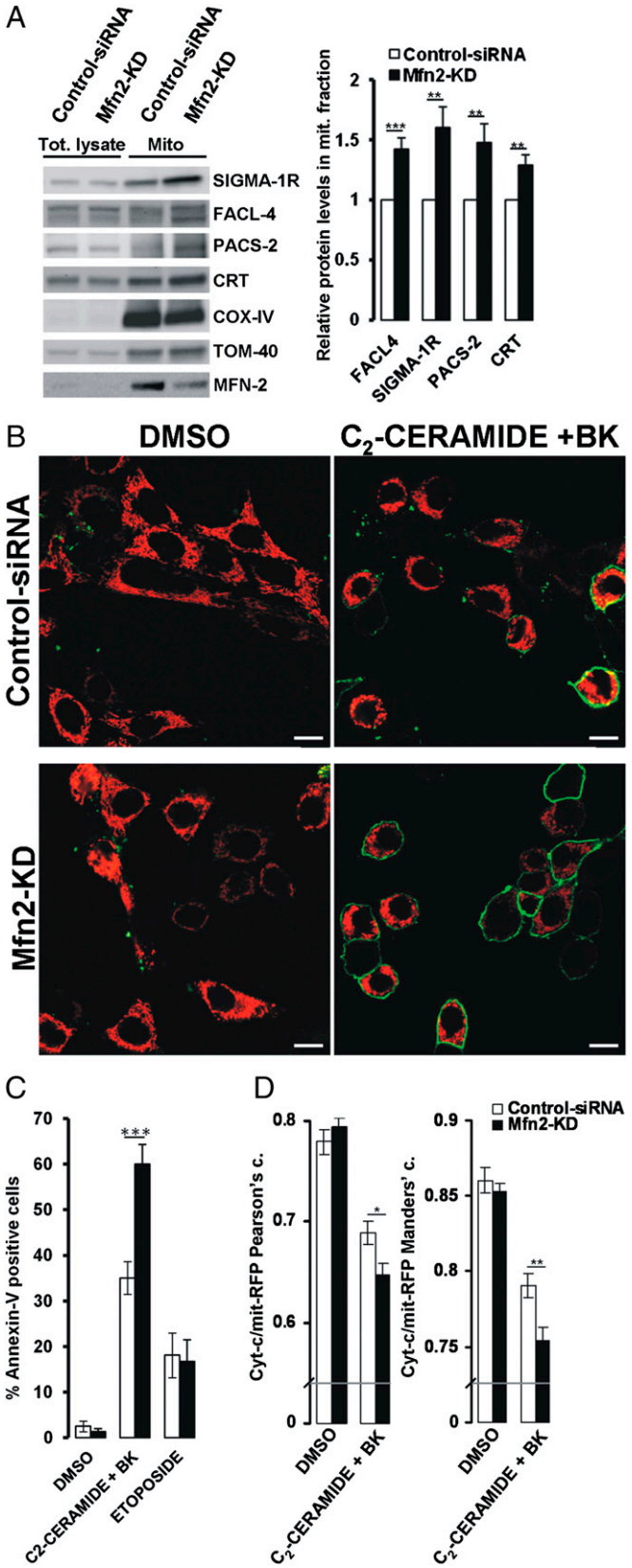

Fig. 6. Mfn2 down-regulation increases ER–mitochondria membrane association and sensitizes cells to mitochondrial Ca^{2+}-dependent death. (*A*) Western blot of the specified proteins in total lysates and crude mitochondrial fractions isolated from the indicated MEFs. The relative protein levels in the mitochondrial fraction were calculated as described in *Materials and Methods*, taking into account their expression level in the total lysate. Data shown represent the mean ± SEM of five different experiments from three independent preparations; $^{**}P < 0.005$, $^{***}P < 0.001$. (*B*) Representative fluorescence images of SH-SY5Y cells cotransfected with mit-RFP and either control siRNA or Mfn2-specific siRNA (Mfn2-KD), treated or not with 40 μM C_2-ceramide + 100 nM bradykinin (BK) (*Materials and Methods*) and stained with Annexin-V-FLUOS (green). (*C*) The percentage of SH-SY5Y$^+$ cells with both mit-RFP and Annexin-V-FLUOS staining treated as in *B* ($n = 4$ independent experiments) or with 60 μM etoposide (*SI Materials and Methods*). Data shown represent the mean ± SEM of three independent experiments; $^{***}P < 0.001$. (*D*) Pearson's and Manders' colocalization coefficients between endogenous cytochrome *c* (*Left*) and mit-RFP (*Right*) signals (*Materials and Methods*) in SH-SY5Y cells of the indicated type treated as described ($n = 36$, 37, 74, and 93 cells for control siRNA + DMSO, Mfn2-KD + DMSO, control siRNA + C_2-ceramide + bradykinin, and Mfn2-KD + C_2-ceramide + bradykinin treatment, respectively). Data shown represent the mean ± SEM; $^{*}P < 0.05$, $^{**}P < 0.01$.

observed both in cardiomyocytes from Mfn2 conditional knockout mice and *Mfn2*$^{-/-}$ MEFs (37). These results are in contrast with our findings demonstrating that acute Mfn2 down-regulation does not significantly modify mitochondrial bioenergetic parameters and suggest that the observed decrease in coenzyme Q results from an adaptation phenomenon to prolonged Mfn2 knockout rather than being a primary effect of Mfn2 ablation.

Based on this evidence, suggesting that Mfn2 cannot contribute to the formation of close contacts between the two organelles since the contacts actually increased upon Mfn2 ablation/reduction, we propose a different role for Mfn2 in ER–mitochondria coupling in which the protein, rather than being a component of the tethering complex, acts as a negative regulator of organelle apposition. However, its action is crucial for cell life, possibly preventing an excess of close contacts between the two organelles that might result in a toxic transfer of Ca^{2+} to mitochondria during cell stimulation (31) and eventually in cell death (38–40).

Our findings demonstrate that the original model for ER–mitochondria tethering, based on Mfn homo/heterodimers with a bimolecular structure of 9 nm (41) (currently widely reported even in review literature; see, for example, refs. 16, 17, 35, and 36), is no longer tenable and needs to be revised. Hints that Mfn2 homo/heterodimers could not be responsible for organelles' tethering were already present in the original paper by Scorrano's group (18): The ER-targeted Mfn2 (Mfn2IYFFT), used by the authors, lacks the HR2 domain at its C-terminal, e.g., the critical domain originally proposed for mitochondrial Mfns' homotypic interactions (41). Moreover, the same authors reported that high-molecular-weight complexes coimmunoprecipitate with Mfn2 (18), thus further suggesting the existence of multimeric/heterogeneous structures bound to the protein. Consequently, the data presented should drive the research community pursuing these themes toward new avenues.

Materials and Methods

Cell Culture and Transfection. MEFs (WT, *Mfn2*$^{-/-}$) were grown as previously described (18), as were SH-SY5Y and HeLa cells (22). All materials were from Sigma-Aldrich unless otherwise specified. MEFs and SH-SY5Y cells were transfected using Lipofectamine 2000 Transfection Reagent (Life Technologies). HeLa cells were transfected using TransIT-LT1 (Mirus Bio). For RNAi experiments, the growth medium was replaced 1 h before transfection with antibiotic-free medium. Control siRNA (MISSION siRNA Universal Negative Control #1 SIC001; Sigma-Aldrich) or Mfn2-siRNA [NM_133201 SASI_Mm01_00027313 (Sigma-Aldrich) for mouse sequences or NM_001127660 SASI_Hs02_00330014 (Sigma-Aldrich) for human sequences] were added to the transfection mixes to a final concentration of 40 nM. RNAi experiments were performed 48 h after transfection.

Aequorin Measurements. Aequorin measurements were carried out as described (22) and are summarized in *SI Materials and Methods*.

Mitochondrial and ER Morphology Analysis. Images for investigating mitochondrial morphology and ER–mitochondria contact sites were taken on a Leica TCS-SP5-II equipped with a PlanApo 100×/1.4 numerical aperture objective.

An argon laser line (488 nm) was used to excite GFP or Alexa Fluor 488, and the signal was collected in the 492- to 537-nm range. RFP was excited by the 543-nm HeNe laser, and its emission was collected in the 555- to 700-nm range. For each image, photomultiplier gain was adjusted slightly to maximize signal and avoid saturation. Once acquired, images were not modified further and were analyzed with ImageJ as detailed in *SI Materials and Methods*.

EM Analysis. For conventional EM, cells were processed as described in *SI Materials and Methods*. For quantification, only regions in which the ER and the OMM proceed in parallel, at a distance <15 nm, for at least the equivalent of the diameter of the examined ER tubule/cisterna were considered to be close contacts.

Cell-Death Assays. SH-SY5Y cells were used for these experiments because the WT MEFs were unexplainably resistant to C_2-ceramide and do not show any sign of apoptosis even at high doses of stimulus (100 μM) and after very long exposure (24 h). For cell-death evaluation, staining of SH-SY5Y cells with annexin-V-FLUOS or cytochrome *c* immunofluorescence was performed as detailed in *SI Materials and Methods*.

Statistical Analysis. All data are representative of at least three different experiments. Data were analyzed using Origin 7.5 SR5 (OriginLab Corporation) and ImageJ (National Institutes of Health). Unless otherwise stated, numerical values presented throughout the text refer to mean ± SEM, n = number of independent experiments or cells; $*P < 0.05$, $**P < 0.01$, $***P < 0.001$. Statistical significance for pairwise comparisons was evaluated with a two-tailed Student's t test.

Details for all of the other experiments performed in this article and any associated references are described in *SI Materials and Methods*.

ACKNOWLEDGMENTS. We thank L. Scorrano for WT and Mfn2$^{-/-}$ MEF lines and Mfn2ActA, Myc-Mfn2 cDNAs; G. Hajnóczky for the cDNAs for the ER–mitochondria linker and OMM-RFP; P. Magalhães for critically revising the manuscript; and C. Fasolato, D. Pendin, and E. Basso for valuable discussions and scientific support. This work was funded by grants from the Italian Ministry of University and Research (to T.P. and P.P.); Grant CPDA109513/10 from the University of Padua (to P.P.); the Fondazione Cassa di Risparmio di Padova e Rovigo (CARIPARO Foundation; Progetti d'eccellenza 2011/2012) (to P.P.); the Veneto Region; the Italian Institute of Technology; the Strategic Projects of the University of Padua; and the Italian National Research Council (to T.P.).

1. Hayashi T, Rizzuto R, Hajnoczky G, Su TP (2009) MAM: More than just a housekeeper. *Trends Cell Biol* 19(2):81–88.
2. Rowland AA, Voeltz GK (2012) Endoplasmic reticulum-mitochondria contacts: Function of the junction. *Nat Rev Mol Cell Biol* 13(10):607–625.
3. Vance JE (1990) Phospholipid synthesis in a membrane fraction associated with mitochondria. *J Biol Chem* 265(13):7248–7256.
4. Rusiñol AE, Cui Z, Chen MH, Vance JE (1994) A unique mitochondria-associated membrane fraction from rat liver has a high capacity for lipid synthesis and contains pre-Golgi secretory proteins including nascent lipoproteins. *J Biol Chem* 269(44): 27494–27502.
5. Bionda C, Portoukalian J, Schmitt D, Rodriguez-Lafrasse C, Ardail D (2004) Subcellular compartmentalization of ceramide metabolism: MAM (mitochondria-associated membrane) and/or mitochondria? *Biochem J* 382(Pt 2):527–533.
6. Contreras L, Drago I, Zampese E, Pozzan T (2010) Mitochondria: The calcium connection. *Biochim Biophys Acta* 1797(6-7):607–618.
7. Pizzo P, Drago I, Filadi R, Pozzan T (2012) Mitochondrial Ca^{2+} homeostasis: Mechanism, role, and tissue specificities. *Pflugers Arch* 464(1):3–17.
8. Szabadkai G, Duchen MR (2008) Mitochondria: The hub of cellular Ca2+ signaling. *Physiology (Bethesda)* 23:84–94.
9. Cárdenas C, et al. (2010) Essential regulation of cell bioenergetics by constitutive InsP3 receptor Ca2+ transfer to mitochondria. *Cell* 142(2):270–283.
10. Glancy B, Balaban RS (2012) Role of mitochondrial Ca2+ in the regulation of cellular energetics. *Biochemistry* 51(14):2959–2973.
11. Bravo R, et al. (2011) Increased ER-mitochondrial coupling promotes mitochondrial respiration and bioenergetics during early phases of ER stress. *J Cell Sci* 124(Pt 13): 2143–2152.
12. Korobova F, Ramabhadran V, Higgs HN (2013) An actin-dependent step in mitochondrial fission mediated by the ER-associated formin INF2. *Science* 339(6118):464–467.
13. Friedman JR, et al. (2011) ER tubules mark sites of mitochondrial division. *Science* 334(6054):358–362.
14. Hamasaki M, et al. (2013) Autophagosomes form at ER-mitochondria contact sites. *Nature* 495(7441):389–393.
15. Westermann B (2010) Mitochondrial fusion and fission in cell life and death. *Nat Rev Mol Cell Biol* 11(12):872–884.
16. Prinz WA (2014) Bridging the gap: Membrane contact sites in signaling, metabolism, and organelle dynamics. *J Cell Biol* 205(6):759–769.
17. Raturi A, Simmen T (2013) Where the endoplasmic reticulum and the mitochondrion tie the knot: The mitochondria-associated membrane (MAM). *Biochim Biophys Acta* 1833(1):213–224.
18. de Brito OM, Scorrano L (2008) Mitofusin 2 tethers endoplasmic reticulum to mitochondria. *Nature* 456(7222):605–610.
19. Cosson P, Marchetti A, Ravazzola M, Orci L (2012) Mitofusin-2 independent juxtaposition of endoplasmic reticulum and mitochondria: An ultrastructural study. *PLoS ONE* 7(9):e46293.
20. Bolte S, Cordelières FP (2006) A guided tour into subcellular colocalization analysis in light microscopy. *J Microsc* 224(Pt 3):213–232.
21. Pla-Martín D, et al. (2013) Silencing of the Charcot-Marie-Tooth disease-associated gene GDAP1 induces abnormal mitochondrial distribution and affects Ca2+ homeostasis by reducing store-operated Ca2+ entry. *Neurobiol Dis* 55:140–151.
22. Zampese E, et al. (2011) Presenilin 2 modulates endoplasmic reticulum (ER)-mitochondria interactions and Ca2+ cross-talk. *Proc Natl Acad Sci USA* 108(7):2777–2782.
23. Giacomello M, et al. (2010) Ca2+ hot spots on the mitochondrial surface are generated by Ca2+ mobilization from stores, but not by activation of store-operated Ca2+ channels. *Mol Cell* 38(2):280–290.
24. Csordás G, et al. (2010) Imaging interorganelle contacts and local calcium dynamics at the ER-mitochondrial interface. *Mol Cell* 39(1):121–132.
25. De Stefani D, Raffaello A, Teardo E, Szabò I, Rizzuto R (2011) A forty-kilodalton protein of the inner membrane is the mitochondrial calcium uniporter. *Nature* 476(7360):336–340.
26. Baughman JM, et al. (2011) Integrative genomics identifies MCU as an essential component of the mitochondrial calcium uniporter. *Nature* 476(7360):341–345.
27. Rojo M, Legros F, Chateau D, Lombès A (2002) Membrane topology and mitochondrial targeting of mitofusins, ubiquitous mammalian homologs of the transmembrane GTPase Fzo. *J Cell Sci* 115(Pt 8):1663–1674.
28. Santel A, Fuller MT (2001) Control of mitochondrial morphology by a human mitofusin. *J Cell Sci* 114(Pt 5):867–874.
29. Huang P, Yu T, Yoon Y (2007) Mitochondrial clustering induced by overexpression of the mitochondrial fusion protein Mfn2 causes mitochondrial dysfunction and cell death. *Eur J Cell Biol* 86(6):289–302.
30. Friedman JR, Webster BM, Mastronarde DN, Verhey KJ, Voeltz GK (2010) ER sliding dynamics and ER-mitochondrial contacts occur on acetylated microtubules. *J Cell Biol* 190(3):363–375.
31. Csordás G, et al. (2006) Structural and functional features and significance of the physical linkage between ER and mitochondria. *J Cell Biol* 174(7):915–921.
32. Hajnóczky G, Csordás G, Madesh M, Pacher P (2000) Control of apoptosis by IP(3) and ryanodine receptor driven calcium signals. *Cell Calcium* 28(5-6):349–363.
33. Giorgi C, et al. (2010) PML regulates apoptosis at endoplasmic reticulum by modulating calcium release. *Science* 330(6008):1247–1251.
34. Ciscato F, et al. (2014) SERPINB3 protects from oxidative damage by chemotherapeutics through inhibition of mitochondrial respiratory complex I. *Oncotarget* 5(9): 2418–2427.
35. Kornmann B (2013) The molecular hug between the ER and the mitochondria. *Curr Opin Cell Biol* 25(4):443–448.
36. Klecker T, Böckler S, Westermann B (2014) Making connections: Interorganelle contacts orchestrate mitochondrial behavior. *Trends Cell Biol* 24(9):537–545.
37. Mourier A, et al. (2015) Mitofusin 2 is required to maintain mitochondrial coenzyme Q levels. *J Cell Biol* 208(4):429–442.
38. Duchen MR (2012) Mitochondria, calcium-dependent neuronal death and neurodegenerative disease. *Pflugers Arch* 464(1):111–121.
39. Nie Q, et al. (2014) Mitofusin 2 deficiency leads to oxidative stress that contributes to insulin resistance in rat skeletal muscle cells. *Mol Biol Rep* 41(10):6975–6983.
40. Wu ZS, et al. (2014) Role of mitofusin-2 in high mobility group box-1 protein-mediated apoptosis of T cells in vitro. *Cell Physiol Biochem* 33(3):769–783.
41. Koshiba T, et al. (2004) Structural basis of mitochondrial tethering by mitofusin complexes. *Science* 305(5685):858–862.